

# The design, manufacture and predicted performance of Kirkpatrick-Baez Silicon stacks for the International X-ray Observatory or similar applications

Richard Willingale and Frank H.P.Spaan

Department of Physics and Astronomy, University of Leicester,  
University Road, Leicester, LE1 7RH, UK

## ABSTRACT

A method of constructing a large aperture grazing incidence X-ray telescope utilizing the Kirkpatrick-Baez (K-B) geometry is described. Two crossed stacks of flat, wedged Silicon plates comprise a single optical unit which provides focusing to a angular resolution limit set by the plate separation within the stacks. If high precision Silicon wafers are used and the focal length is large, an angular resolution of a few arc seconds is achievable. As a refinement an angular resolution at the limit imposed by the K-B geometry could be met if the plates were very slightly curved to the correct parabolic profile along the axial direction. A tessellation of a large number of identical or nearly identical stacks over a spherical aperture plane can provide a very large collecting area and high angular resolution suitable for the International X-ray Observatory (IXO) or similar X-ray astronomy applications. The optical design operates in a similar way to the lobster eye geometry and unlimited extension of the aperture coverage (tessellation) can provide a very large field of view suitable for all-sky monitoring.

**Keywords:** X-ray optics for astronomy

## 1. INTRODUCTION

For the next generation of X-ray telescopes we need a technology that can provide large collecting areas of several square meters at  $\sim 1$  keV and an angular resolution of a few arc seconds or better. An ideal scheme would be modular in which the large primary aperture is populated by a tessellation of many identical or near identical units. Each unit would achieve the required angular resolution and provide a small fraction of the total area. Suitable mutual co-alignment of the units renders the all-up angular resolution, and dense packing of the units provides high aperture utilization and ultimately the large collecting area required. To implement such a scheme we need an optical design which is amenable to such modularization and we need a method of manufacture that can meet the tolerances required for the angular resolution and a mechanical construction that provides high aperture utilization with as little mass as possible.

One of the ways to focus X-rays is to use the Kirkpatrick-Baez (K-B) set-up.<sup>1</sup> Recently a suggestion was made to apply this design to the mirror concept of the International X-ray Observatory (IXO) by using stacks of Silicon plates.<sup>2</sup> The Silicon stacks are manufactured in exactly the same way as the Silicon pore optic stacks proposed for implementation of the Wolter I (W-I) geometry by Beijersbergen et al.,<sup>3</sup> an example of which is shown in Fig. 1 left. For the K-B set-up, each perpendicular square pair of stacks makes up one module (Fig. 1 centre). A constellation of such modules can then be made to fill the mirror area using, for example, a filling rule known in botany to be used by the sunflower, which can be shown to have the closest packing<sup>4</sup> (Fig. 1 right). In this arrangement the rays are deflected towards the corner of each module as indicated by the diagonal lines. Each module is aligned so that the maximum collecting area is achieved at the centre of the field of view.

Another way of focusing X-rays has been pointed out by Angel<sup>5</sup> which is similar to the way the eye of a lobster is built. In the lobster mirror design, tubes or pores with a square cross-section are positioned on a sphere; each pore has its axis pointing to the centre of the sphere. Two reflections off adjacent sides of the square pore bring the radiation to a focus on a spherical surface concentric with the aperture sphere and half the radius. Any point in the heavens can be imaged this way; there is no limit in the field of view and there is no axis of

---

E-mail: rw@star.le.ac.uk, fs78@star.le.ac.uk

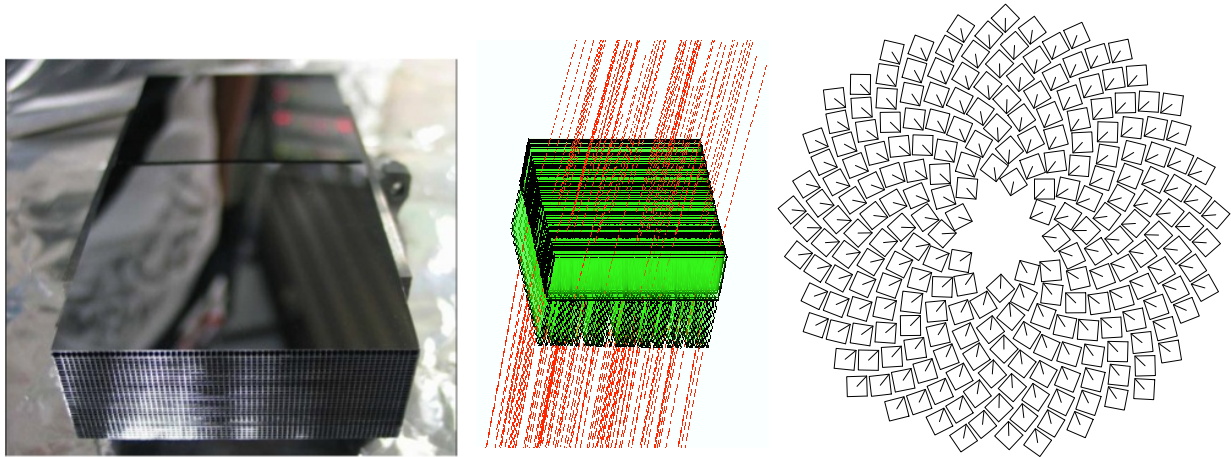


**Figure 1.** Left: A W-I type of module made of stacked Silicon plates. Centre: two stacks of Silicon plates making up a K-B module. Right: a tessellation of such modules based on the sunflower configuration which uses Fibonacci numbers. The lines from the centre to the corner of each module indicate the direction in which 2-reflection rays are deflected.

symmetry for the optical system. Given a particular point source, a certain fraction of the pores will focus the rays; the rest will not play a role because of vignetting as the grazing angle (with respect to the axis of the pore) is too large. The resolving power of this system is limited by the width of the pores, and also by diffraction if the wavelength is long. The ratio of the length to width of the pores determines the effective area and the level of stray light arising from rays which pass through the pores without reflection.

This paper investigates combining elements of these two imaging techniques.

## 2. THE PRINCIPLE

In the new design, we start from a spherical lobster geometry in which the pores are replaced by the K-B modules. The placement of the front and back stacks for one module is schematically shown in Fig. 2. The module is positioned on the sphere and the tapering angle is dictated by the line to the centre of curvature which is positioned at twice the focal length. The front and back stacks have slightly different focal lengths. When the plates are all planar, the resolution of the system is determined by the pore size (or by diffraction if the wavelength is long). What is not assessed in this paper, but follows from the usual K-B characteristics, is that using curved plates instead of flat ones can improve the resolution; the required axial curvature along the plates is very small.

The alignment requirements for this system are different from those for the Silicon pore W-I design, where the inter-alignment within a module is crucial. In the new design, each stack has well defined radial axes. Such axes are straight lines which lie along the plane reflecting surfaces of both the front and back stack. The only critical alignment is that these axes all pass through a single point, the centre of the sphere. There are many possible axes within a K-B pair of stacks but because the plates are tapered, all these axes will pass through the centre of the sphere. Rotation of the stack about any axis is totally unimportant, as is translation of the stack tangentially over the surface of the sphere. Providing the axes of every stack are aligned to a common centre the integrity of the image and angular resolution are secure.

The distribution of rotations of the stacks within the tessellation that fills the aperture dictates the effective area that will be associated with certain positions on the sky. This is because the maximum efficiency is reached when the angles of incidence for the two reflections in the module are the same. The sunflower tessellation shown in Fig. 1 is designed to maximize the area for a particular sky position, i.e. the pointing direction of the telescope or the centre of the field of view, because the modules are placed with their diagonal toward the optical axis. In general a tessellation of K-B stacks has no axis of symmetry (unlike a W-I system which has) but the arrangement of the stacks does change the vignetting and the distribution of the collecting area over the

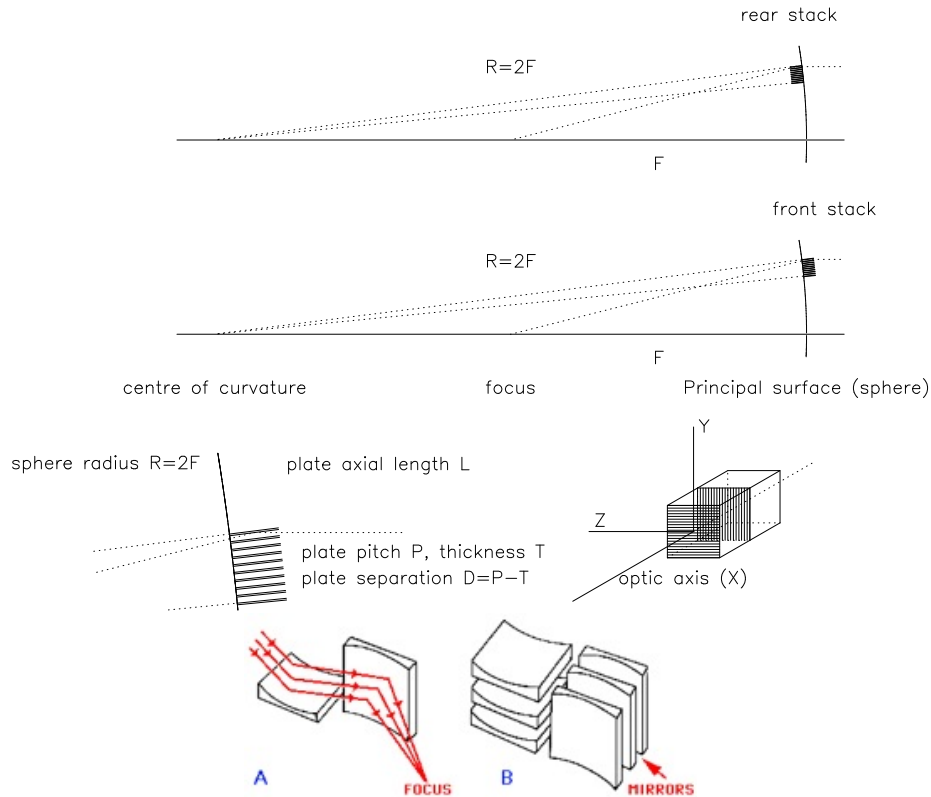


**Figure 2.** Top: The set-up of K-B Si stacks on a spherical principal surface. Centre: the tapering requirement of the individual plates, and the perpendicular stack arrangement within one module in three dimensions. Bottom: Kirkpatrick-Baez with curved plates to improve the resolution.

field of view. In the sunflower tessellation the diagonal lines across the aperture faces of the stacks all point to a common centre, the centre of the aperture. Some alternative tessellation might seek to achieve the opposite of this such that no point in the field of view was targeted for a high area. In such a tessellation the distribution of rotation angles would have to be random or quasi random with respect to any particular potential centre.

Application of this design to the IXO or similar X-ray telescope can provide a larger field of view than is possible with the W-I geometry. If the field of view is modest (a few degrees or less) then the modules need not be placed on a sphere but, as is more conventional, we can use the tangential plane. The modules can be packed in a Cartesian grid and the telescope is much the same as the *LAMAR*<sup>6,7</sup> concept. Because the Si plates are nominally planar and the plate separation,  $D$ , is constant the maximum collecting area on-axis is achieved using an axial plate length,  $L$ , that is inversely proportional to radius within the aperture,  $r$ ,  $L = 2DF/r$  (see Fig. 2). As with the W-I Si pore optic design,<sup>3</sup> the modules must be longer in the centre of the aperture than at the outer edge. If the modules are identical with a fixed axial length  $L$  then we will produce a response closer to the *LAMAR* with a flatter vignetting.

### 3. SIMULATION OF THE PERFORMANCE

In this section two and three dimensional simulation results are described. The former are meant to illustrate the principle; the three dimensional results aim to investigate the performance of a realistic system.

#### 3.1. Results of two dimensional simulations

In our first simulation, an array of 25 mirrors is placed such that they have their centres on a part of a circle (see fig. 3 top-left). Opposite each mirror an absorbing surface is placed, and between these structures, which represent

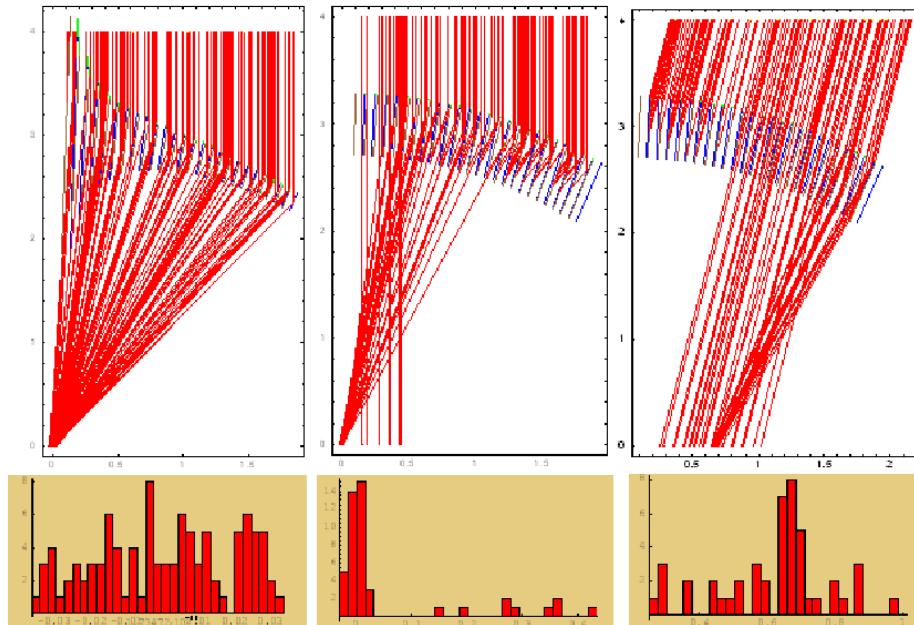


**Figure 3.** Top left: rays are focused by a set of mirrors with different axial lengths positioned on a circle. Bottom left: the histogram of ray counts in the detector plane. Top and bottom centre: idem but with mirrors having a fixed axial length. Top and bottom right: idem but with the light source at a different angular position. Note that the x-scales of the histograms are not equal and that the left histogram shows that this system has an on axis resolution of one pore width as expected.

the pores, there is another more or less horizontal absorbing surface. Each mirror is set at the appropriate angle for focusing, and the appropriate axial length for field of view and vignetting: rays coming in at some off-axis angle  $\alpha$  are all focused; the width of this focus is determined by the pore width. In Fig. 3 top-centre the mirror lengths have been fixed to 1/4 of the previous maximum value; this leads to some rays passing through pores without reflection (stray rays, for small mirror angles) and to some pores showing vignetting (for larger mirror angles). This behavior of the optic is the same for each ray angle, an example is shown in Fig. 3 top-right. In the lower part of Fig. 3 the respective histograms of the detector counts are shown.

Fig. 4 left shows the same situation as in Fig. 3 top-centre, except that the mirrors have been shifted into the  $z = R_0$  line, along their radius to the centre of the circle, while keeping the mirror angle the same. The response is almost identical but the configuration less demanding for integration. For imaging a small field of view the form of the aperture surface is not important. We used a circle for Fig. 3 and a line for Fig. 4. Line focusing to the limit set by the plate separation is achieved providing plates are set at the correct taper angles. In these simulations 123 randomly placed rays were used and the reflectivity of the mirrors has been included in intensity calculations (not in the histograms, which show detector hit counts), based on 1 keV and Iridium.

In Fig. 4 centre binned intensities are shown for different values of  $\alpha$  (0, 5, 10 deg), 1234 rays were used and a fixed mirror size of 1/2 of the previous maximum size. Despite the stray rays the source position can be extracted (note this is a linear plot). In Fig. 4 right the situation is shown for  $\alpha = 10$  degrees, illustrating the different pore regions: the central pores transmit rays without reflection, the pores on the right part of this area focus properly, and the pores left and right of that area block the rays.

Note that the reflectivity (efficiency) is very poor for large angles, but equals 1 for rays going through without reflection. Therefore the stray light is emphasized (which is correct in this two dimensional case). The distribution of the reflection grazing angles onto the mirrors for each off-axis angle  $\alpha$  is similar.

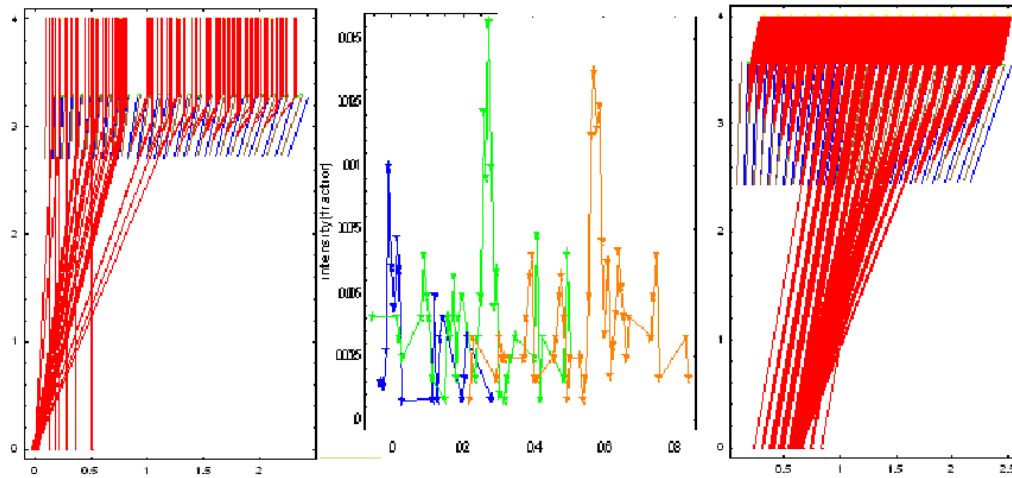


**Figure 4.** Left: as in Fig. 3 top-centre, but now with the mirrors in the  $z = 3$  plane. Centre: using this configuration, the intensity on the detector for three different values of  $\alpha$ : 0, 5 and 10 deg. Right: an illustration of the different parts of the optic for an off axis source (see text).

### 3.2. Results of three dimensional simulations

The two dimensional results have shown some of the characteristics of the design; the three dimensional results described in this section are taken from a full three dimensional simulation of an optic similar to that required for the IXO. The focal length is  $F = 20$  m, the energy 1 keV, the reflective material Iridium, the mirror aperture radius runs from 0.25-1.90m, the Silicon plate width is 100mm, the plate separation distance (equivalent to the pore width) is  $D = 0.610$ mm. The sunflower constellation of K-B modules is used in the mirror plane, and for each module the wedge angle of the plates is calculated such that proper focusing takes place. The axial length of the reflective surfaces is kept constant over the whole mirror.

An example of the rays in the aperture plane is shown in Fig. 5, with a point source at about 100 arcmin off axis; a part of the mirror aperture is active in focusing the rays from that source while the rest of the mirror blocks the rays because the grazing angles are too large. In the top-left of the Fig. 5 rays hitting the mirror that eventually reach the detector are shown lighter, the others darker. In the top right part of the Fig. all the rays are shown. The plot bottom-left shows the detector distribution as a logarithmic three dimensional graph and bottom-right as an image of detector counts. The cruciform shape of the image arises from the single reflection rays brought to a line focus by the front and rear stacks. The same occurs for the Angel-lobster eye optics.

When the axial lengths of the plates vary inversely with radius in the aperture we get the optimum utilization of the reflecting area for a source on-axis and the optical characteristics as already shown.<sup>2</sup> Fig. 6 top-left shows the radial surface brightness distributions for a sequence of  $\alpha$  from 0 to 3 degrees in 1/2 degree steps. For  $\alpha = 0$  only 1 point is visible; on this scale the surface brightness is like a  $\delta$ -function. For the next three  $\alpha$ s the peaks are clearly visible (note this is a logarithmic plot) and for the last values no peak is distinguishable from the stray light noise level.

The angular resolution is 5 arcseconds Half Energy Width (HEW) and is independent of off-axis angle  $\alpha$ . This is a little smaller than the ratio  $D/F$  which is geometrically the expected full width of the line focus produced by each stack.

On the top-right of Fig. 6 is the vignetting function for focused rays only (arbitrary normalization). The detected distribution for  $\alpha = 30$ arcmin is shown below that as a three dimensional image on a logarithmic scale. As has been shown in the two dimensional analysis, fixing the mirror lengths leads on the one hand to more

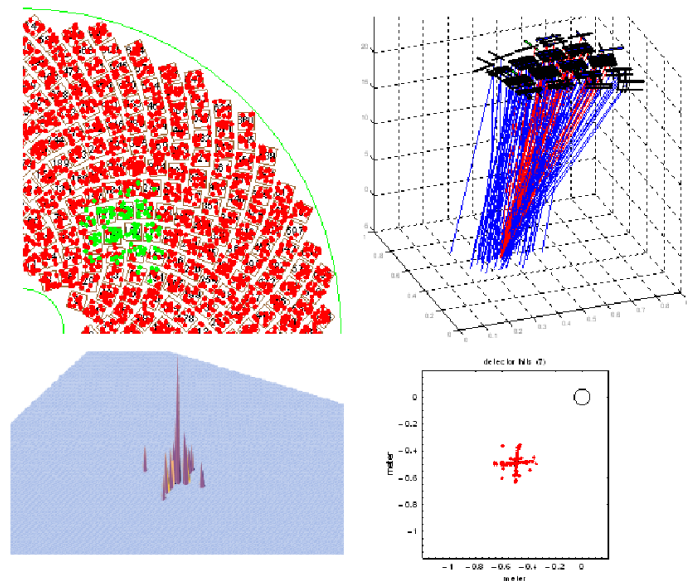


**Figure 5.** Top left: distribution of rays across the mirror tessellation for an off-axis source. Rays that hit the detector are shown lighter. Top right: for the same situation all rays and active plates are shown. Bottom left and right: the corresponding detector distribution. In the right-hand plot the black circle indicates the relatively small field of view of the wide field imager currently under consideration for IXO.

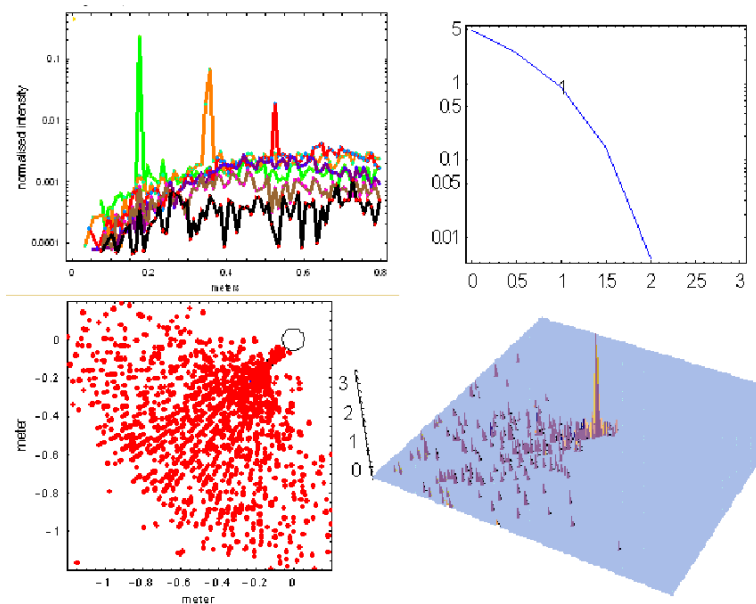


**Figure 6.** Top left: the surface brightness as a function of the distance from the centre of the field for different  $\alpha$ . Bottom left and right show examples of the detector image for  $\alpha = 0.5\text{deg}$ . Top right shows the effective area as a function of the viewing angle in degrees; only focused rays have been considered.

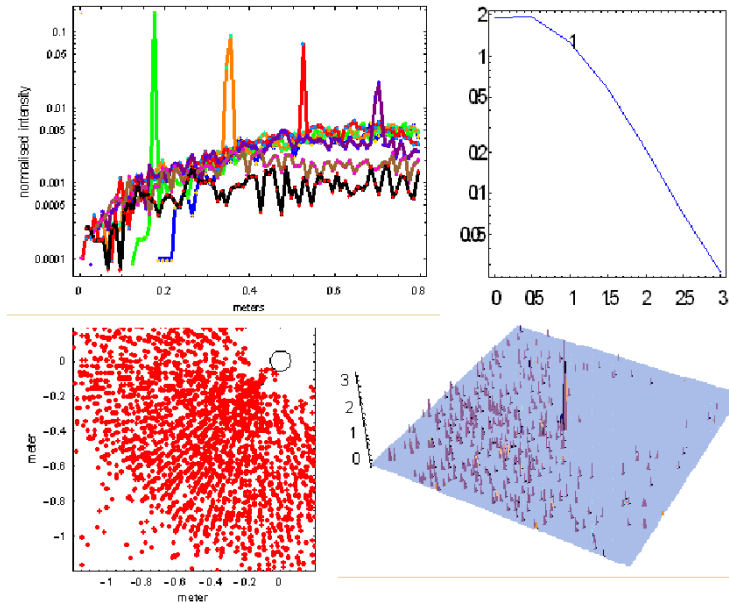


**Figure 7.** As in Fig. 6, but now for a fixed mirror length of 1/8 of the maximum of the variable lengths. In the top-left part of the figure the on axis point spread function starts with a sharp peak, only visible as one point, beyond about 0.2m the stray light of this curve starts to emerge (not distinguishable when printed in gray shades).

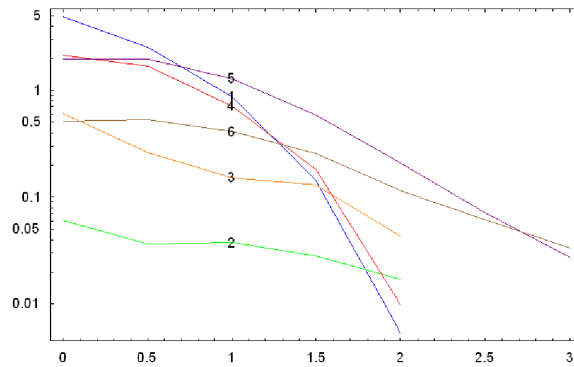


**Figure 8.** The vignetting function based on focused rays for different values of the mirror length.

stray light, but on the other hand to a larger field of view. This is illustrated in Fig. 7 where the length is fixed to 1/8 of the maximum length in the case of varying lengths. Compared with Fig. 6, we see the row of peaks continue into areas of larger  $\alpha$  (Fig. 7 top left), while the stray light noise level does not change very much. The pattern of the stray light has changed as can be seen by comparing Fig. 6 bottom-right and Fig. 7 bottom-right, for a fixed mirror length the noise is spread both more evenly and over a large area.

The vignetting function for variable and fixed axial length designs are plotted in Fig. 8. Curve 1 corresponds to variable mirror lengths, curve 2 has the longest fixed length, 6 the shortest. There is clearly an optimal value for the fixed mirror length depending on the application criteria. This Fig. also shows that beyond  $\alpha=3$  degrees imaging of the source is still possible. The K-B design can provide a useful field of view which is much larger than required for the current concept of IXO,  $\approx 0.17$ deg.

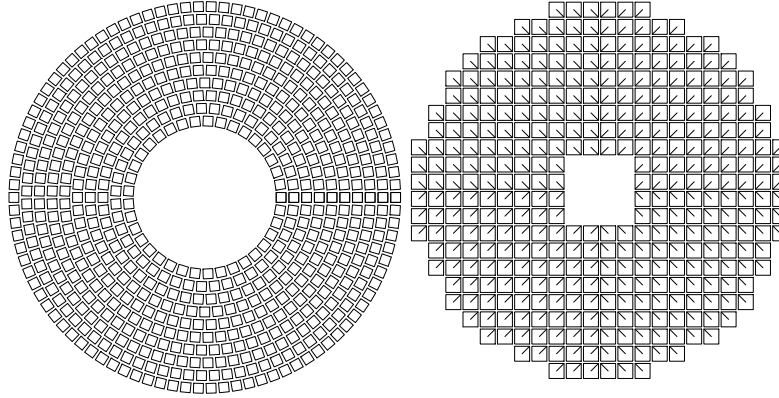


**Figure 9.** Left: radial packing of modules used for the W-I design. Right: The simple cartesian packing used as an alternative to the sunflower tessellation for the K-B design.

Geometry	tessellation	$L$ mm	A m <sup>2</sup> at 1 keV	$\alpha_{50}$ degrees	$A\alpha_{50}^2$
W-I	radial	variable	3.70	0.212	0.166
W-I	radial	44	2.40	0.213	0.109
K-B	sunflower	variable	2.41	0.392	0.370
K-B	sunflower	24	1.48	0.550	0.448
K-B	cartesian	variable	1.06	0.558	0.330
K-B	cartesian	24	0.74	0.733	0.397

**Table 1.** Comparison of the on-axis collecting area and the width of the vignetting function at 1 keV for different W-I and K-B configurations. The rightmost column is a figure of merit for wide field instruments.

#### 4. COMPARISON OF W-I AND K-B SILICON PORE OPTICS

In order to compare the optical performance of W-I and K-B Si pore optics we have used the IXO baseline parameters described above and used ray-tracing to estimate the on-axis collecting area at 1 keV and the off-axis angle at which vignetting function at 1 keV drops to 50% of the on-axis value,  $\alpha_{50}$ . We have assumed that the structure required to mount the modules in the aperture has a fixed blocking factor,  $f_{struc} = 0.4$ , a value which can probably be achieved by careful design and optimization. For both optical designs the axial length of the plates can be varied inversely as a function of radius or can be fixed. The tessellation used for the W-I was a radial packing as shown in Fig. 9. For the W-I design there is no option for rotating the modules wrt to the radius vector. Two tessellations were considered for the K-B design, the sunflower arrangement shown in Fig. 1 and the simple cartesian packing shown in Fig. 9. Table 1 shows the results. The fixed values of axial length  $L$  were chosen to maximise the on-axis area.

For an instrument which is primarily designed to provide the highest sensitivity for isolated target sources maximising the collecting area at the centre of the field of view is the highest priority. Clearly the W-I configuration with variable  $L$  is best. This is the baseline for IXO. However for an instrument designed to find faint, serendipitous point sources or survey work or imaging extended sources like SNRs or clusters of galaxies then the size of the field of view is important. A useful figure of merit is  $A\alpha_{50}^2$  which is roughly proportional to the grasp of the telescope. This is shown as the rightmost column in Table 1. All the K-B configurations considered have a significantly higher figure of merit than the W-I configurations. For the IXO f-ratio (aperture size c.f. the focal length) considered the sunflower tessellation with fixed  $L$  is slightly better than the others but the advantage is not large. If the focal length were shorter and/or the aperture were larger then the simple K-B configuration with cartesian packing and fixed  $L$  would be advantageous for wide field applications.

For both the W-I and K-B designs the limiting angular resolution is set by the pore size  $D = 0.610$  mm. For the W-I the point spread function is slightly more peaked with HEW = 3.7 arcseconds on-axis but this degrades to HEW = 5 arcseconds at an off-axis angle of 20 arcminutes. The point spread function for the K-B design

remains constant at HEW=5 arcseconds independent of the off-axis angle.

## 5. CONCLUSIONS

An X-ray telescope that combines aspects of the K-B and Angel-lobster designs and can be constructed using stacks of Silicon plates leads to an optic with properties somewhat different from the more common W-I configuration. Both the K-B and W-I Si pore optics provide an angular resolution which is limited by the pore size when the axial profile of the plates is straight. If a small axial curvature can be introduced, approximating to the parabolic-hyperbolic surfaces of a W-I or a parabolic surface for the K-B then the angular resolution can be improved. For the W-I design the angular resolution degrades off-axis but for the K-B design it is constant, independent of source position. The K-B design has a wider vignetting function than the W-I design and the maximum field of view that can be covered is not limited by the grazing angles. K-B modules can be added to the outer edge of the aperture without limit. As a larger area of the spherical principal surface is covered the field of view on the spherical image surface increases in the same way as for the Angel-lobster design. Note that there is no lateral inversion in the image plane for the K-B design.

The choice of the mirror concept for the IXO has to take into account many parameters; the angular resolution, the collecting area (both as a function of source angle and energy), the manufacturability and the alignment procedure. The K-B design cannot match the on-axis collecting area of the W-I design and has a lower high energy response because the grazing angles are  $\approx \sqrt{2}$  larger. However, the K-B Si stacks are probably easier to construct than for the W-I because the plates don't have to be curved (and therefore they are not stressed) and it is likely that an angular resolution which is closer to the theoretical limit can be realised using the K-B optics. The W-I Si optics are the preferred choice providing the stacks can be made with the tolerances required to meet the limits of the angular resolution. The K-B Si stacks provide an alternative solution with a reduced on-axis collecting area but wider field of view and comparable angular resolution.

K-B Si optics are better suited to wide field applications. They offer the potential for high angular resolution combined with large collecting area and unlimited field of view; the next generation of all-sky X-ray monitor. The optics for such an instrument can be constructed using a tessellation of completely identical K-B Si stack modules and the technology for manufacturing these modules exists.

Further investigation is required to ascertain the angular resolution limit that can be achieved by introducing axial curvature in the plates (and including diffraction) and to quantify the level of stray light as a function of pore size, axial plate length and X-ray reflectivity (X-ray energy).

## REFERENCES

1. Kirkpatrick, P. and Baez, A.V., 1948, J. Opt. Soc. Am. 38, 766-773
2. Spaan, F., Willingale, R., Optimisation of the X-ray optics for IXO, American Astronomical Society 213th meeting.
3. Beijersbergen, M., Kraft, S., Günther R., Mieremet, A., Collon, M., Bavdaz, M., Lumb, D. and Peacock, A., 2004, Proc SPIE Vol. 5488, 868-874
4. Vogel, H., 1979, Mathematical Biosciences, 44:179-189
5. Angel, J.R P., 1979, ApJ, Part 1, vol. 233 p. 364-373
6. Cohen, L.M., Fabricant, D.G., Gorenstein, P., 1986, Proc SPIE, Vol. 691, p. 126-137
7. Fabricant, D., Cohen, L., Gorenstein, P., 1987, Applied Optics, 27, 1456